
Separation Science and Technology
Publication details, including instructions for authors and subscription information:
http://www.tandfonline.com/loi/lsst20

# Theoretical Modeling and Numerical Simulation of Axial-Vortex Separation Technology Used for Oily Water Treatment

Yipeng Ji[ba], Jiaqing Chen[b], Xiangdong Jiao[b], Xiaolei Cai[ab] & Pei Li[ab]
[a] Beijing University of Chemical Technology, Chaoyang, Beijing, 100029
[b] Beijing Institute of Petrochemical Technology, Daxing, Beijing, 102617
Accepted author version posted online: 23 Apr 2015.

# Theoretical Modeling and Numerical Simulation of Axial-Vortex Separation Technology Used for Oily Water Treatment

Yipeng Ji[a, b*], Jiaqing Chen[b], Xiangdong Jiao[b], Xiaolei Cai[a, b], Pei Li[a, b]

a. Beijing University of Chemical Technology, Chaoyang, Beijing, 100029

b. Beijing Institute of Petrochemical Technology, Daxing, Beijing, 102617

**Abstract:** The Voraxial Separator (VAS) has attracted increasing attention in recent years because it can separate large volumes of oily water efficiently within a tubular compact structure. However, there is a lack of systematic research into the working mechanism and validation of the design theory of the separation technology. In this paper, the key factors influencing the separation efficiency of the VAS were analyzed, the theoretical model of this new separation technology was established, and a pilot VAS was designed. The velocity field in the pilot VAS was also analyzed by numerical simulation, which could provide a useful reference for the theoretical research. The results show that the tangential velocity distribution at the swirler end is in accordance with the pattern of Solid Body vortex, and there exists a low pressure region along the central longitudinal flowline which can be proved by the distribution of axial velocity. The maximum separation efficiency of the pilot VAS can achieve is up to 93%, which occurs when the back-flow ratio is 2.9-11.4%.

**Keywords:** Voraxial Separator; oil-water separation; theoretical model; numerical simulation

# 1. Introduction

As the production life of oilfields extend longer and longer, the water content in the well stream becomes increasingly higher and is now generally more than 80%. The increase in the water content results in the heavier load of oily water treatment facilities. Based on current oil production worldwide, a total of 300 million barrels of water needed to be treated every day in 2013, of which up to 80 million barrels come from offshore platforms (1). Treatment of oily water produced in oilfields has become a bottleneck hindering the further development of offshore oilfields. How to achieve efficient oil-water separation with simple and compact equipment has become a hot topic in the oil and gas industry (2). Therefore, compact and tubular separation equipment with high efficiency has attracted a great deal of attention and is being studied extensively (3).

Unfortunately, only a few tubular separation apparatus such as the rotary cyclone and liquid-liquid hydrocyclone (LLHC) have been developed for oily water treatment to date (4, 5). The rotary cyclone was designed by TOTAL CFP Inc. and NEYRTEC Inc. as early as in 1984 (6). The structure of rotary cyclone is relatively complex, and the vibration of a long rotating drum is unavoidable, therefore, the oil stream concentrated at the axial central line is unstable. Compared with the LLHC, the rotary cyclone has not been widely used in oil-water separation facilities up to

now. However, the LLHC has some disadvantages. For example, the diameter of a single LLHC is so small that it cannot be directly tied into the pipelines to achieve in-line separation in practice. The range of operation parameters for LLHC must be strictly controlled to maintain high separation efficiency. The tangential inlet of the oily water will no doubt result in an asymmetric vortex and large pressure drop (7-9). In 1996, Dirkzawger designed the axial inlet hydrocyclone (AIH), which has been developed into the engineered products known as In-line hydrocyclone and In-line Dewater owned by the FMC Technologies in recent years (10). Because the vortex is generated by guide vanes, the pressure drop and shearing stress in the AIH is much lower than that in the LLHC. However, the diameter and working capacity of single AIH are still relatively small, and the range of operation parameters are narrow (5).

In the middle of 1990s, Enviro Voraxial Technology (EVTN) Inc. in United States produced a new separation device named the Voraxial Separator (VAS), which integrates centrifugal force and axial lift force within a tubular apparatus (11-13). In terms of working principle, it is an axial vortex separation technology. The internal swirler can produce a strong vortex to match the large diameter of the static barrel and can also be adjusted. In 2004, EVTN conducted a successful experiment on an offshore oil platform in the Gulf of Mexico (GOM). In 2010, after the GOM oil spill disaster, British Petroleum (BP) purchased several custom-designed VASs from EVTN for surface floating oil recovery (14). It has been demonstrated that VAS achieves separation

efficiencies up to 95-100% when separating free oil from water. It also has the advantages of low energy consumption and a compact footprint, only 37 kW and 4$m^2$ respectively, at a treatment capacity of 1135 $m^3$/h (9, 11, 15). However, no intensive research or thorough analysis of the working mechanism for this new type of separation technology has been performed, so it lacks a solid theoretical foundation for wide application in different working conditions. Therefore, starting from vortex motion theory, a simplified design model for axial vortex separation technology is developed, and a new pilot VAS analysis method is independently put forward in this paper. Finally, commercial Computational Fluid Dynamics (CFD) software is employed to conduct numerical simulation on this pilot VAS.

# 2. Mechanistic Modeling

## 2.1 Conceptual design

Taking the centrifugal force and axial lift force into consideration simultaneously within a tubular apparatus, the conceptual design scheme of VAS is illustrated in Fig. 1. The VAS mainly consists of three components, that is, the swirler, the static barrel, and the light phase collection pipe, among which the swirler and the static barrel are the critical parts. Along the axial flow direction, the whole VAS can be divided into three sections with different fluid flowing state, i.e., the accelerating section, the steady state section and the disperse-phase concentrating section.

### 2.1.1 Swirler

The swirler has a significant impact on the separation performance and determines the initial swirl intensity. It can be generally divided into the following four types: rotary-drum type, tangential-injection type, static fixed-vane type and dynamic propeller type (16-18). The rotary-drum type swirler is widely used in centrifuge separators and rotary cyclones. When the drum rotates at a high speed, the oily water in it will also rotate at the same speed to form a vortex. The angular velocity of the drum can be controlled conveniently by adjusting the treatment load and the oily water properties. In the tangential-injection type and static fixed-vane type swirlers, the vortex can be produced by means of changing the velocity. In running processes, they do not need a driver and therefore are widely used in some separators with ultra-compact space requirements such as LLHC and AIH. In the dynamic propeller type swirler, the vortex is induced by the revolving blades. High-speed rotary blades can produce very high shearing stress at the gap between the static barrel wall and the blades themselves, it is therefore rarely used for oily water treatment.

To ensure that the swirler's angular velocity can be controlled conveniently for specific working conditions, the swirler of VAS is designed based on the concept of rotary-drum and dynamic propeller type swirlers. The main structure of the swirler is a drum which inner surface is welded with certain number of helical blades and the blades play a similar role in dynamic propeller. The

axial length of the helical blades is shorter than the drum, and the drum can be divided into a fluid accelerating section and the fluid steady state section. During the working process, the oily water enters the swirler from the left and first encounters the accelerating section, where a vortex is produced by the rotary drum together with the continuous helical blades. The tangential velocity distribution is similar to the rotation of a rigid body and thus can be abbreviated as a solid body vortex (19-21).

A cylindrical coordinate system is established shown in Fig. 1. An oil droplet with diameter $d_o$ located at radius $r$ within the vortex will experience centripetal force $F_p$ and drag force $F_d$, which can be given by

$$F_p = \frac{\pi}{6} d_o^3 \frac{u_\theta^2}{r} (\rho_w - \rho_o) \quad (1)$$

$$F_d = \frac{1}{2} C_D \rho_w V_{sr}^2 \frac{\pi d_o^2}{4} \quad (2)$$

$$u_\theta = \omega r \quad (3)$$

where $u_\theta$ is the tangential velocity of the oily water, $\omega$ is the angular velocity of the blades, $\rho_w$ is the density of continuous water phase, $\rho_o$ is the density of dispersed oil phase, $V_{sr}$ is the radial slip velocity of the oil droplet relative to continuous water phase, and $C_D$ is the drag coefficient. It

should be noted that $C_D$ depends on Reynolds number, which is 0.44 as the Reynolds number is greater than $10^5$ (22, 23).

According to Eq. (1) and (2), if the angular velocity is constant, the centripetal force acting on the oil droplet will decrease with *r*, while the drag force is unrelated to the location of the oil droplet. When *r* is small, the centripetal force will be less than the drag force; this region is called the dead zone, where the heavy phase cannot flow out and the light phase is prohibited from converging toward the central axis (24). To avoid the impact of the dead zone on separation efficiency, most of the previous studies have adopted different methods to evacuate the internal the liquid of the central region (10, 24-27). However, those methods will inevitably cause liquid mixing at different tangential and axial velocities and the vortex motion is disturbed.

The blades are designed to have a solid-body height less than the drum radius. The fluid accelerating section is divided into the outer-ring blade region and the central hollow region. The direction of relative velocity of the liquid at any point in the outer-ring blade region vs the solid-body blade is consistent with tangential direction of the blades. With $u_z$ representing the axial velocity, the absolute velocity *v* in this region can then be given by

$$\vec{v} = \vec{u_\theta} + \vec{u_z} \quad (4)$$

The flow rate to be treated with the VAS is denoted by $Q$, the inner radius of the drum is denoted by $R$, and the average initial axial velocity $\overline{u_{z0}}$ can be given by

$$\overline{u_{z0}} = \frac{Q}{\pi R^2} \quad (5)$$

Considering the rotating continuous helical blades will work like an axial pump and the formula for the theoretical lift coefficient $C_{y0}$ of the blades is given by

$$C_{y0}\frac{l}{t} = \frac{2\Delta u_\theta}{\omega_\infty}\sin\beta_\infty \quad (6)$$

where $l$ is the circumference of the drum, $t$ is the number of the blades, $\omega_\infty$ is the inflow velocity, $\beta_\infty$ is the angle between the inflow velocity and the axial line, and $\Delta u_\theta$ is the tangential velocity component of liquid. According to Eq. (4) and (6), the increment of the mean axial velocity component of the liquid in the outer-ring blade region $\Delta u_z^{'}$ can be expressed as

$$\Delta u_z^{'} = C_{y0}\frac{u_\theta}{\tan\phi} = C_{y0}\frac{\omega r}{\tan\phi} \quad (7)$$

where $\phi$ is the helical blade's lead angle. If the impact of the centrifugal force on the axial velocity is ignored, the increment of the flow rate in the outer-ring blade region $\Delta Q$ can be given by

$$\Delta Q = \int_{r_{ce}}^{R} \Delta u_z \pi r \eta dr = C_{y0}\frac{\pi^2\omega}{3\tan\phi}(R^3 - r_{ce}^3)\eta \quad (8)$$

where $\eta$ is the transport efficiency of the helical blades, $r_{ce}$ is the radius of the central hollow region. It should be mentioned that, when the flow rate in the outer-ring blade region is increased by the pumping effect of the helical blades, the pressure head in this region will be increased also. From Eq. (8), it can be seen that, when the angular velocity of the blades $\omega$ is large enough, the pressure head resulted by the helical blades will large enough to overcome the energy loss occurred in the static barrel. Therefore, "zero pressure loss" of the oil-water separation can be realized from the inlet to the outlet. According to the principle of mass conservation, the mean axial velocity $u_{zc0}$ in the central hollow region at the outlet of the swirler can be expressed as

$$u_{zc0} = \frac{Q - \Delta Q - \frac{Q}{\pi R^2}(R^2 - r_{ce}^2)}{\pi r_{ce}^2} \quad (9)$$

From Eq. (9), it can be demonstrated that, the decrease of the initial mean axial velocity $u_{zc0}$ of liquid in the central hollow region means that the liquid at this region is sucked out. If $u_{zc0}$ is less than zero, the liquid at this region is flow reversely of that in the outer-ring blade region, therefore the corresponding pressure will be zero or negative. Obviously, the central hollow region of low pressure will be formed, which will effectively avoid the dead zone without causing any disturbance of the vortex motion.

### 2.1.2 Static barrel

The static barrel coaxial with the swirler is connected to the outlet end of the steady state section and the light-phase collection pipe is mounted at the end of the static barrel on the same axial line. After flowing through the swirler, the light phase and heavy phase gradually separate in the static barrel, the light phase concentrates around the axial central line and then it is collected by the light-phase collection pipe. The vortex on the inner wall of the static barrel is called the "vortex tube". The total vorticity in the "vortex tube" constantly declines due to vortex dissipation. The major factors affecting the vortex dissipation ratio for a finite-boundary tubular pipe are the Reynolds number, vortex type and initial vortex strength.

Eq. (1) states that the centripetal force acting on the light-phase droplet is in direct proportion to the square of its tangential velocity. If it is possible, reducing the decay amplitude of the tangential velocity under the condition of no external energy input will improve the separation efficiency. According to the principle of conservation of angular momentum, when the vorticity is constant, the diameter of the "vortex tube" decreases, and both the tangential velocity and axial velocity of liquid inside the vortex will increase. One convenient method to reduce the diameter of the "vortex tube" is to reduce the diameter of the static barrel by adopting an internal continuous conical shape (26, 28, 29). Therefore, the static barrel of VAS is designed with a conical shape. The relationship

between the tangential velocity $u_\theta$ and axial velocity $u_z$ of the liquid inside the cone-shaped pipe and the radius of the cone tube can be given as follows (19),

$$u_\theta = u_{\theta 0}(\frac{d_i}{d})^2 \quad (10)$$

$$u_z = u_{z0}(\frac{d_i}{d})^2 \quad (11)$$

where $u_{\theta 0}$ and $u_{z0}$ are the initial values of the tangential velocity and axial velocity respectively, while $d_i$ and $d$ are the maximum diameter of the cone-shaped pipe and the diameter of the observation point respectively.

## 2.2 Velocity analysis of the liquid in static barrel

### 2.2.1 Axial Velocity

The axial velocity of liquid in the cone-shaped static barrel can be expressed in terms of a cubic function of the radius $r$ (19, 23, 27), i.e.

$$u_z(r) = a_1 r^3 + a_2 r^2 + a_3 r + a_4 \quad (12)$$

where $a_1$, $a_2$, $a_3$ and $a_4$ are constants.

The appropriate boundary conditions can be given to determine the above four constants,

a. The velocity in the center of low pressure region is considered as constant, so,

$$u_z(r = r_c) = u_{zc} \tag{13}$$

b. The velocity is maximum at the wall,

$$\frac{du_z(r = R)}{dr} = 0 \tag{14}$$

c. The velocity in the center of the low pressure region is considered as the minimum value,

$$\frac{du_z(r = r_c)}{dr} = 0 \tag{15}$$

d. the flow inside the VAS obeys the law of mass conservation,

$$2\pi\rho\int_{r_{ce}}^{R} u_z(r) r dr + u_{zc}\pi\rho r_c^2 = \overline{u_z}\pi\rho R^2 \tag{16}$$

where $\rho$ is the density of multiphase liquid, $u_{zc}$ is the mean axial velocity in the central low pressure region, $r_c$ is the radius of the center of low pressure region. Considering the effect of cone shape, the value of these two parameters can be taken as follows,

$$u_{zc} = \overline{u_{z0}}[(\frac{d_0}{d})^2 - 1] \tag{17}$$

$$r_c = r_{ce}\frac{d}{d_0} \tag{18}$$

### 2.2.1 Radial Slip Velocity

The radial slip velocity $V_{sr}$ of oil droplet relative to continuous water phase which is closely associated with the lift force, centripetal force and drag force acting on the oil droplet in the vortex flow (30). Comparatively speaking, the lift force has large effect on an oil droplet with a small diameter ($d_o \le 10\mu m$). Since the VAS does not possess the separation ability for the oil droplet with diameter $d_o \le 10\mu m$, here only the impact of drag force and centrifugal force are taken into consideration while ignoring the lift force, and $V_{sr}$ can be calculated according to the famous Stokes formula as

$$V_{sr} = [\frac{4}{3}(\frac{\rho_w - \rho_o}{\rho_w})\frac{d_o \cdot u_\theta^2}{C_D \cdot r}]^{\frac{1}{2}} = [\frac{4}{3}(\frac{\rho_w - \rho_o}{\rho_w})\frac{d_o \cdot \omega^2 r}{C_D}]^{\frac{1}{2}} \qquad (19)$$

## 2.3 Separation efficiency

If the radius of the light-phase collection pipe is denoted by $r_l$, and the radius within which all oil droplets can reach $r_l$ is denoted by $r_{crit}$, the separation efficiency of oil droplets with a given diameter $d_o$ can be expressed as the ratio of the area within which the oil droplets are separated to the total area of liquid flow. This method has also been applied by other researchers (23, 27). The separation probability for oil droplet of any given diameter $\varepsilon(d)$ can therefore be expressed as

$$\varepsilon_{ff}(D)=\begin{cases}0 & if \quad r_{crit}=r_l \\ \dfrac{\pi(r_{crit}^2-r_l^2)}{\pi(R^2-r_l^2)} & if \quad r_l<r_{crit}<R \\ 1 & if \quad r_{crit}=R\end{cases} \tag{20}$$

The total separation efficiency for various dispersed particle size in oily water is given by

$$\varepsilon_{ffu}=\frac{\sum_j \varepsilon(d_j)V_j}{V} \tag{21}$$

where $V_j$ is volume of light phase with particle diameter is $d_j$ and $V$ is the total volume of light phase.

# 3. Preliminary structural design

Based on the above theoretical analysis, a pilot VAS was designed with a VAS geometry shown in Fig.2. This pilot mainly consists of a inlet, driving mechanism, cylindrical drum, continuous helical blades, cone-shaped static barrel and light-phase collection pipe. The driving mechanism actually comprises a motor, a synchronous belt and a pair of gear transmission. Only the gear transmission is illustrated in Fig.2, and the final large gear is essentially manufactured together with the cylindrical drum. Two continuous helical blades are welded at the inlet-side of the cylindrical drum inner wall, which length is smaller than that of the drum and its height is smaller than the inner radius of the drum. The cone-shaped static barrel is fixed at the outlet end of the drum along the same central axis, and the light-phase collection pipe is rigidly bonded on the outlet

end of the static barrel. When the motor is started, the cylindrical drum would be driven through the driving mechanism.

## 3.1 Continuous helical blades

According to Eq. (9), when the axial velocity of liquid in the central hollow region is less than zero, the back-flow rate $Q_r$ and its ratio (ε) to total flow rate $Q$ in the central hollow region are respectively given by

$$Q_r = Q - \frac{Q}{R^2}(R^2 - r_{ce}^2) - \Delta Q \tag{22}$$

$$\varepsilon = \frac{Q_r}{Q} \tag{23}$$

According to Eq. (22), (23) and (8), the total flow rate $Q$, the radius $r_{ce}$ of the central hollow region, the angular velocity of the cylindrical drum $\omega$ and the lead angle of the helical blades at the outlet $\Phi$ are key parameters controlling the back-flow ratio. The radius of the central hollow region is closely related to the flow rate and the rotary velocity of the drum. Therefore, a preferable design should be done for a specific application. When the flow rate at the given the radius of the central hollow region and the angular velocity of the cylindrical drum are constants, the lift force acting on liquid tends to increase with the decrease of the blade lead angle. To keep the incoming stream flow at steady state, the lead angle of helical blades at inlet is set to 90°, and then it is reduced

gradually along the axial length of blades. Regardless of their thickness, the unfolded pattern of the blades at the maximum diameter looks like a parabola which is shown in Fig. 4, and the equation for the unfolded line can be given as

$$x = a\zeta^2 + b\zeta \tag{24}$$

where $a$ and $b$ are constants, $\xi$ is the lengthwise direction of unfolded helical blades, and $x$ is the direction of inner drum's unfolded line. If we assume that the lead angle of helical blades is $\alpha$ when the axial distance from inlet is $l$, then the cotangent of the lead angle $\alpha$ can be expressed as

$$\cot\alpha = \frac{dx}{dz} = 2az + b \tag{25}$$

If the lead angle of helical blades at the outlet is set to $\Phi$, and its total axial length is set to $L$, considering the fact that the lead angle of helical blades at inlet has been set to 90° previously, we can get the value of $a$ and $b$ respectively as follows according to Eq. (25),

$$b = 0 \tag{26}$$

$$a = \frac{\cot\Phi}{2L} \tag{27}$$

## 3.2 Cone-shaped static barrel

The length of the static barrel is determined by the hydraulic retention time(HRT) needed for the separation process. The longest time needed for light-phase oil droplet to move from the wall surface of static barrel to the central axial region is

$$\tau = \int_{r_l}^{R} \frac{18\mu_w r}{d^2(\rho_w - \rho_o)u_\theta^2} dr = \frac{18\mu_w}{d^2(\rho - \rho)w^2}(\ln R - \ln r_l) \quad (28)$$

where $\tau$ is the separation time, $\mu_w$ is the viscosity of continuous phase. Thus, the required static barrel length $L$ should be

$$L \geq \tau \overline{u_z} \quad (29)$$

The conical angle is obviously another key parameter of the static barrel. Using similar separation equipment such as LLHC and AIH as a design reference, we can see that a double-cone or single-cone contour is conventionally used for LLHC, a single-cone contour with conical angle less than 10° is taken for LLHC (31-33), and the conical angle is 11° of the AIH barrel (34). Here the preliminary conical angle of the static barrel is taken as less than 10° for VAS. Of course, the value of conical angle needs to be determined based on more comprehensive considerations for specific conditions.

# 4. Numerical Simulation

Although various factors affecting the separation efficiency have already been considered as thoroughly as possible based on the theoretical model mentioned above, there are still some limitations in predicting the internal flow field of VAS by analytical methods, and it is therefore important to find other means to validate the model. It has been proven through many studies that numerical simulation of the vortex motion process for the tubular equipment can be executed by using commercial CFD software, which can provide significant guidance for the detailed structural design of some critical structure parts (35-37).

The CFD numerical simulation method has been widely adopted in developing hydrocyclones whose separation process is similar to that of the VAS to some extent, and the simulation results have already been recognized as valid and acceptable in the industry (38-41). Therefore, a three-dimensional numerical simulation is performed on the separation process of VAS by ANSYS FLUENT14.5 software package in this study. The tangential velocity and axial velocity of the liquid in the cone-shaped static barrel and the separation efficiency of different oil droplet size are calculated, and the relationship between separation efficiency and the theoretical back-flow ratio is then analyzed.

## 4.1 Geometry and meshing

The pilot VAS was designed to handle 1$m^3$/h oily water, and the split ratio, which is the ratio of the volumetric flow rate of the light-phase collection pipe to the inlet feed stream, was pre-determined to be 5% for the present numerical simulation. The inner diameter of the cylindrical drum is 25 mm, and its length is 100 mm. The lead angle of blades at the outlet is 66.400°, the length is 60 mm, the thickness is 3 mm and the height is 7.5 mm. The length of the static barrel is 320 mm, the conical angle is 0.896°, and the inner diameter at inter-connection side is 25 mm. The inner diameter of the light-phase collection pipe is 10 mm.

The whole geometry is split into five blocks and each block is then meshed separately in Gambit integrated in the software package. The interface between each block is denoted as "interface". The zone of the swirler is defined as the “Frame Motior” zone with an angular velocity of 3500rpm. The “moving wall” boundary condition is used for wall boundary in the swirler section and its angular velocity is defined relative to the adjacent cell zone. The wall of the inlet and the static barrel and the light-phase collection pipe are all fixed as non-slipping walls. Check on the grid independence were carried out through five different mesh densities with cell numbers varying from 1,000,000 to 4,000,000 for the same physical model. Four of them achieved convergence; of course, longer convergence time is needed for higher mesh densities. For the sake of compromise

between accuracy and computational time, the computational domain is finally divided into 1,395,775 hexahedral cells, and the skewness factor is less than 0.62.

The physical properties of oily water are based on the produced water drained from one three-phase separator in Zhongyuan Petroleum Exploration Bureau under the Sinopec Group. At a temperature of 20℃, the density and viscosity of the produced water are 1.1 g/cm$^3$ and 1.47 mPa·s, respectively. The density of the corresponding crude oil is 0.86 g/cm$^3$, and its viscosity is greater than 5.4 mPa·s. The oil content at the inlet feed stream is pre-determined to be 1278 mg/L, and the average particle size of oil droplets is taken as 50μm.

## 4.2 Simulation methodology

The flow field inside a VAS can be characterized as an inherently unsteady, highly anisotropic turbulent field in a confined, strongly swirling flow. Although time-dependent turbulence approaches such as Large Eddy Simulation (LES) or Direct Numerical Simulation (DNS) should be used for such conditions, these techniques are computationally intensive and are not practical for many industrial applications (41). The $k$-$\varepsilon$ renormalization group (RNG) model, the Reynolds Stress Model (RSM) and the $k$-$\varepsilon$ model have been independently used to evaluate the flow field and separation performance under a comprise between accuracy and computational time (8, 33, and 42-44). Considering the fact that the RSM model can successfully address the rapid changes of

stream-lined curvature, vortex, rotation and tension force, as well as achieving high precision for the complex flow-field simulation, it was chosen for the numerical simulation of the VAS in this paper. The detailed fundamental equations can be found in the ANSYS FLUENT software user manual (45).

The numerical simulation is carried out using a 3-D segregated steady-state double-precision implicit solver. A pressure interpolation scheme named PRESTO (pressure staggered option) is adopted, which has been reported to be very useful for predicting swirling flow characteristics prevailing inside the cyclone body (40). To obtain the pressure field inside the system, the SIMPLE (semi-implicit pressure linked equations) algorithm scheme is preferred, which uses a combination of continuity and momentum equations to derive an equation for pressure. Interpolation of field variables from the cell centers to faces of the control volumes is generated with the higher-order quadratic upwind interpolation (QUICK) spatial discretization scheme (40).

## 4.3 Related analysis, results and discussion

### 4.3.1 Analysis of velocity

#### (1) Tangential Velocity

As the effects of the boundary layer and energy loss have been neglected, the theoretical value of tangential velocity can be calculated by Eq. (3), and the change in tangential velocity can be found

by Eq. (10). The distribution of the numerical simulation and theoretical values of the tangential velocity on the barrel cross section at distances from swirler outlet of 50 mm, 100 mm, 150 mm, 200 mm, 250 mm and 300 mm are shown in Fig. 5. It can be observed from the distribution of the numerical simulation value that the position of maximum tangential velocity decreases gradually from the wall to the center. This shows that the vortex pattern translates correspondingly from an solid body vortex to a concentrated vortex, which is a combination of a forced vortex near the VAS axis and a free vortex near the wall region.

In forced vortex region, the theoretical and numerical simulation values are in good agreement. It is demonstrated that there is scarcely any eddy dissipation in the forced vortex region. The maximum tangential velocity decreases with the increase of the distance from swirler outlet caused by the friction-induced energy loss near the boundary. For example, the maximum tangential velocity is 2.8 m/s at a distance of 50 mm from the swirler outlet, and it becomes 2.4 m/s at a distance of 300 mm from the swirler outlet, the total decrease is 14.3%. However, the energy loss near the boundary is neglected in theoretical model and the distribution of tangential velocity gets from the theoretical model is consistent with that in the forced vortex. Therefore, when the point of interest is away from the inner wall of static barrel, the theoretical tangential velocity matches the CFD simulation result very well, but it seems not to be so well when the point of interest locates in the region near the boundary. The eddy dissipation increases with the distance from the swirler

outlet, and the tangential velocity error between theoretical model and the CFD model increases too.

**(2) Axial Velocity**

As the effects of the boundary layer and energy loss are neglected, and the velocity in the center of low pressure region is set to be constant, the theoretical value of the axial velocity can be calculated by Eq. (12) - (18). The distribution of the axial velocity by numerical simulation and theoretical model in the static barrel cross section at a distance from the swirler outlet of 50 mm, 100 mm, 150 mm, 200 mm, 250 mm and 300 mm are shown in Fig. 5. It can be observed that, the distribution of theoretical and numerical simulation values of axial velocity are in good agreement except Fig 5. (a). As shown in Fig 5, when the distance from the swirler outlet is greater than 50 mm, there is no back flow in the static barrel. However, the axial velocity in the central region is very low. The radius of the low velocity range is approximately 5 mm at the distance of 50 mm from the swirler outlet, which is equal to the radius of the central hollow region of the swirler. The radius of the low velocity range is less than 3 mm at a distance of 300 mm from the swirler outlet, the decreased value is directly proportional to the decreased radius value of the static barrel. As to the value of absolute axial velocity, because of the cone-shaped effect of the static barrel, it increases gradually, especially in central region. For example, the value of the axial velocity in the

central region is 0.2 m/s at a distance of 50 mm from the swirler outlet, and it increases to 0.4 m/s at a distance of 300 mm from the swirler outlet, which means an increase of nearly two fold.

In theoretical model, the velocity is assumed to approach maximum at the wall, and the energy loss in boundary layer is also ignored. Hence in the region near the wall, the axial velocity got from theoretical model is bigger than that from CFD model. Being different from the tangential velocity, the energy loss near the wall has only a little effect on axial velocity. Therefore, the theoretical axial velocity matches the CFD model very well in the vicinity of the wall region.

In the central region of the static barrel, the initial axial velocity got from Eq. (9) is zero, but it is 0.2m/s according to the numerical simulation result shown in Fig. 5(a). The axial velocity error between the theoretical model and the CFD model is perhaps mainly caused by the simplifying assumption of Eq. (9). Considering the flow inside the VAS obeys the law of mass conservation, when there is a big error between theoretical model and the CFD model of the axial velocity in the central region of the static barrel, the error near the wall will also be correspondingly big, which can be found in Fig. 5(a) and (b). If it is possible, we can concentrate on improving the accuracy of Eq. (9) in the future.

### 4.3.2 Effect of oil droplet size

The minimum oil droplet size that can be efficiently separated is a key factor of the separation performance of the pilot VAS. During the process of theoretical prediction, the static barrel is considered as a cylinder, and the diameter of oil droplet is set to the average particle size used in numerical simulation. Now, the theoretical separation efficiency can be calculated by Eq. (19), (20) and (21). Fig.6 shows the theoretical and simulation separation efficiency with oil droplet sizes ranging from 20μm to 70μm with a 10μm interval. It can be seen that, the two kinds of values coincide with each other when average oil droplet size is greater than 40μm. The separation efficiency is higher than 80% under this condition. When the average oil droplet size is less than 40μm, the separation efficiency decreases rapidly, and it can fall below 50% if the average oil droplet diameter is less than 30μm. Furthermore, there is a lager error between the values of the two analyses under this condition, which may be caused by the assumption that the static barrel is of cylindrical shape in theoretical model. As shown in Fig 6, the cone-shaped static barrel can effectively increase the separation efficiency of oil droplet with small diameter.

### 4.3.3 Effect of back-flow ratio

The VAS can effectively avoid the dead zone with the lift force generated by the helical blades in the central hollow region and the back-flow rate in the low pressure region is the key operating

factor affecting the separation efficiency. As shown in Eq. (8), (19) and (20), the back-flow rate increases with the decrease of the inlet flow and increases with the increase of the rotary velocity of the drum. The separation efficiency of the pilot VAS at different back-flow rates is simulated under the same treatment load and other parameters, with results shown in Fig. 7. It can be inferred that the highest separation efficiency, which can reach 93%, occurs when the back-flow ratio is 2.9-11.4%.

### 4.3.4 The relationship between pressure and velocity

The low pressure region caused by the pumping effect of the rotary helical blades is the key to avoid the dead zone. The distribution of pressure and axial velocity at the outlet of swirler were calculated by CFD model and theoretical model respectively, with results shown in Fig. 8. It can be observed that the value of pressure and axial velocity at the outlet of swirler reduce with the decrease of the static barrel radius. The results match the analysis of 2.2.1 very well that the pumping effect caused by the rotary helical blades can increase the pressure and axial velocity in the outer-ring blade region and at the same time can suck liquid out of the central hollow region. When the liquid is sucked out, the low pressure and low axial velocity will be formed in the central hollow region and which can avoid dead zone effectively.

# 5. Conclusions

(1) The significant structural features of VAS can be described as that, the swirler is actually a rotary drum with two helical blades bonded on its inner circumferential surface, the light-phase collecting section adopts a slightly cone-shaped static barrel connected after the swirler. As the VAS starts to work, the fluid within the swirler is driven by the rotary drum and helical blades, and axial vortex is generated with low shear stress. At the same time, with the positive pumping effect of the helical blades, the increased pressure head can not only overcome the energy loss occurred in the static barrel, but also suck some liquid radial outward from the central hollow region. Therefore, less static pressure at inlet is needed for the oily water to be treated, and the light phase is more flexible to transfer towards the central hollow region without influencing the vortex state.

(2) A theoretical model for the separation process of VAS is established based on forced vortex theoretical, according to the characteristics of the VAS swirler. The theoretical model can be used to analyze the key parameters that influence the back-flow ratio in the central region of swirler, to solve the unfolded profile equation for the helical blade, and to calculate the axial and tangential velocity in the light-phase collecting section of VAS. According to the proposed theoretical model, the minimum length of static barrel can be calculated based on the required HRT, and the separation efficiency can also be calculated for difficult diameter oil droplet.

(3) To investigate the interior flow condition among differential areas and qualify the specific velocity at a random position within the VAS, the flow field in VAS is numerically simulated by the commercial CFD software package. The results show that, the tangential velocity distribution at the outlet of swirler conforms to the law of forced vortex, and it is significantly influenced by the friction-induced energy loss near the wall in the static barrel. The maximum value of tangential velocity decreases with the increase of distance from the swirler outlet, but its value remains unchanged in the vortex core area far away from the wall of the static barrel. The diameter of vortex core area deceases with the increase of distance from the swirler outlet, and the type of vortex is gradually transformed from a solid-body vortex to a concentrated vortex. However, the friction-induced energy loss near the boundary has only a little effect on the axial velocity, the maximum and minimum value of axial velocity appears in the near wall region and in the central hollow region respectively. Under the cone-shaped effect of the static barrel, the axial velocity in the central region grows with the increase of the distance from swirler outlet, while the diameter of the low axial velocity region decreases with the increase of the distance from swirler outlet.

(4) Comparing between the results of the CFD simulation model and theoretical model, it can be seen that, they are in well agreement for tangential velocity at the region far away from the wall. However, the obvious deviation of tangential velocity between two models occurs in the region near the wall and it grows significantly with the increase of distance from the swirler outlet. At the

same time, the results of the CFD simulation model and theoretical model are also in well agreement for axial velocity at the region away from the swirler with a distance bigger than 100mm. The deviation of axial velocity between two models appears primarily near the swirler, and it decreases with the increase of distance from the swirler outlet. Therefore, the theoretical model can be used as a reliable design criterion for the VAS primarily, while the CFD simulation model can be used to verify the separation efficiency more accurately and to qualify the specific velocity value. Of course, the CFD simulation model can also be used in the future to carry out the optimum design of some key parts of VAS.

(5) Besides the inherent structural parameters of VAS, the operating parameters such as the rotary speed and flow rate of VAS and the physical properties of oily water to be treated will also absolutely influence the separation performance. The separation efficiency of pilot VAS under different oil droplet diameter and back-flow ratio in the central area has been attempted either by the theoretical model or by the CFD simulation model just for an “effective exposure”. It is demonstrated simultaneously by the theoretical model and the CFD simulation model that, the highest separation efficiency, which can reach more than 84.4%, occurs when the diameter of oil droplet is greater than 40μm. While the CFD simulation model shows that the separation efficiency approaches the maximum when the back-flow ratio is 2.9-11.4% with oil droplet of 50μm.

## Acknowledgments

The authors would like to acknowledge the financial support provided by the National Natural Science Foundation of China (No. 51079006) and the Funding Project for Academic Human Resources Development in Institutions of Higher Learning under the Jurisdiction of Beijing Municipality (No. PHR201107213).



## References

1. Fakru'l-Razi Ahmadun; Alireza Pendashteh; Luqman Chuah Abdullah; Dayang Radiah Awang Biak; Sayed Siavash Madaeni; Zurina Zainal Abidin.(2009) Review of technologies for oil and gas produced water treatment. J. Hazard. Mater., 170 (2-3): 530-551.

2. M. J. H. Simmons; E. Komonibo; B. J. Azzopardi; D. R. Dick.(2004) Residence time distributions and flow behaviour within primary crude oil-water separators treating well-head fluids. Chem. Eng. Res. Des., 82 (10): 1383–1390.

3. A.L.S. Souza; M.W. Figueiredo; C. Kuchpil; M.C. Bezerra; A.G. Siqueire; C.A. Furtado.(2005) Water management in Petrobras: Developments and challenges. The 2005 Offshore Technology Conference held in Houston. 2-5 May 2005 OTC17258.

4. R. Schook V. van Asperen. (2005) Compact separation by Means of inline technology. The 14th SPE Middle East Oil & Gas Show and Conference held in Bahrain International Exhibition Centre. 12-15 March 2005 SPE 93232.

5. R. Schook; D. Thierens.(2011) De-bottlenecking of mature field production through the use of very compact and efficient separation equipment, topside or subsea. The 2011 Offshore Technology Conference held in Houston. 2-5 May 2011 OTC21617.

6. Triponey G; Woillez J; Bezard C.(1992) The rotating de-oiling cyclone: Recent Development and Operating Experience. The 1992 European Petroleum Conference held in Cannes. 16-18 November 1992 SPE25034.

7. Colman D A; Thew M T.(1983) Correlation of separator result from light dispersion hydrocyclone. Chem. Eng. Res. Des., 61: 233~240.

8. J.P. Veerapen; B.J. Lowry; M.F. Couturier.(2005) Design methodology for the swirl separator. Aquacult. Eng., 33 (1): 21-45.

9. A. Gupta; R. Kumar.(2007) Three-dimensional turbulent swirling flow in a cylinder: Experiments and computations. Int. J. Heat Fluid Flow. 28 (2): 249~261.

10. S. J. Kegge.(2000) Numerical simulation of an axial hydrocyclone. M. Sc. Thesis, Delft University of Technology.

11. Alberto Di Bella; Michael M. Anthony. Apparatus with Voraxial Separator and analyzer. US Patent. No. 6248231B1, Jun. 19, 2001.

12. Harvey E. Richter; N. Palm Beach, Fla. Method and apparatus for separation fluids having different specific gravities. US Patent. No. 5084189, Jan. 28, 1992.

13. A. DiBella; M. Anthony. Voraxial filtration system with self-cleaning auxiliary filtration apparatus. US Patent, No.7727386 B2, Jun. 1, 2010.

14. Chris Sheldon.(2004) Separator tested for use in offshore oil production, http://www.filtsep.com.

15. Perry A. Fischer. (2005) New type of water separator could help fill multiple oilfield needs. Word Oil, 12: 49~52.

16. R. Hreiz; C. Gentric; N. Midoux.(2011) Numerical investigation of swirling flow in cylindrical cyclones. Chem. Eng. Res. Des., 89 (12): 2521~2539.

17. Akay A. Islek.(2004) The impact of swirl in turbulent pipe flow. M. Sc. Thesis, Georgia Institute of Technology.

18. W. Steenbergen; J. Voskamp.(1998) The rate of decay of swirl in turbulent pipe flow. Flow Meas. Instrum., 9 (2): 67–78.

19. A. F.Moene.(2003) Swirling pipe flow with axial strain experiment and large eddy simulation. Ph.D Thesis, Technische Universiteit Eindhoven.

20. O. Lucca-Negro; T. O'Doherty.(2011) Vortex breakdown: a review, Prog. Energy Combust. Sci., 27 (4): 431-481.

21. W. Peng; A.C. Hoffmann; H.W.A. Drries; M.A. Regelink; L.E. Stein.(2005) Experimental study of the vortex end in centrifugal separators: The nature of the vortex end. Chem. Eng. Sci., 60 (24): 6919-6928.

22. Jose G. Severino; Luis E. Gomez; Shoubo Wang; Ram S. Mohan; OvadiaShoham.(2009) Mechanistic modeling of solid separation in solid/liquid hydrocyclones. The 2009 SPE Annual Technical Conference and Exhibiton held in New Orleans. 4~7 October 2009 SPE 124499.

23. G. Carlos; C. Juan; W. Shoubo; G. Luis, M. Ram; S. Ovadia.(2001) Oil-Water separation in Liquid-Liquid Hydrocyclones (LLHC)-experiment and modeling. The 2001 SPE Annual Technical Conference and Exhibition, New Orleans, 4-7 October 2001, SPE 124499.

24. Tetsuya Yamaoto; Natsuko Watanabe; Kunihiro Fukui; Hideto Yoshida.(2009) Effect of inner structure of centrifugal separator on particle classification performance. Powder Technol., 192 (3) 268~272.

25. Q. Gao.(2011) Evolution of eddies and packets in turbulent boundary laers. Ph.D. thesis, the University of Minnesota.

26. J.J. Seureau; Yves Aurelle; M.E. Hoyack.(1994) A Three-phase separator for the removal of oil and solids from produced water. The SPE Annual Technical Conference and Exhibiton held in New Orleans. 25~28 September 1994 SPE 28535.

27. S. Amini; D. Mowla; M. Golkar; F. Esmaeilzadeh.(2012) Mathematical modeling of a hydrocyclone for the down-hole oil–water separation (DOWS), Chem. Eng. Res. Des., 90 (12): 2186-2195.

28. Kuo-Jen Hwang; Y. Hwang; Hideto Yoshida; Kazuha Shigemori.(2012) Improvement of particle separation efficiency by installing conical top-plate in hydrocyclone. Power Technol., 232 (0): 41-48.

29. Kuo-Jen Hwang; Ya-Wan Hwang; Hideto Yoshida.(2013) Design of novel hydrocyclone for improving fine particle separation using computational fluid dynamics. Chem. Eng. Sci., 85 (0) 62-68.

30. Takuro Kouda; Yoshimichi Hagiwara.(2006) An experimental study on turbulent swirl water flow with immiscible droplets. Int. J. Heat Fluid Flow, 27 (4): 611~618.

31. Wang Li-yang, Zheng Zhi-chu, Wu Ying-xiang, Guo Jun, Zhang Jun, Tang Chi.(2009) Numerical and experimental study on liquid-solid flow in a hydrocyclone, J. Hydrodyn, 21: 408-414.

32. A. Davailles; E. Climent; F. Bourgeois.(2012) Fundamental understanding of swirling flow pattern in hydrocyclones, Sep. Purif. Technol., 92: 152-160.

33. Y.R. Murthy; K.U. Bhaskar.(2012) Parametric CFD studies on hydrocyclone. Powder Technol., 230: 36-47.

34. R. Delfos, S. Murphy, D. Stanbridge, Ž. Olujić, P.J. Jansens.(2004) A design tool for optimizing axial liquid-liquid hydrocyclones, Miner Eng., 17: 721-731.

35. R.M. Alkhaddar; P.R. Higgins; D.A. Phipps; R.Y.G. Andoh.(2001) Residence time distribution of a model hydrodynamic Voraxial Separator. Urban Water. 3 (1-2):17-24.

36. F. Sotiropoulos; Y. Ventikos.(2001) The three-dimensional structure of confined swirling flows with vortex breakdown. J. Fluid Mech., 426:155~175.

37. F.M. Erdal.(2001) Local measurements and computational fluid dynamics simulations in a gas liquid cylindrical cyclone separator. Ph.D. Thesis, the University of Tulsa.

38. S. Shi; Y. Wu; J. Zhang; J. Guo; S. Wang.(2010) A study on separation performance of a vortex finder in a liquid-liquid cylindrical cyclone. J. Hydrodyn. Ser. B, 22 (5) 391-397.

39. M.A. Reyes; J.E. Pacheco; J.C. Marín; L.R. Rojas; J. Rincón.(2006) Numerical simulation and experiments of the multiphase flow in a liquid-liquid cylindrical cyclone separator. Proceedings of European Fluids Engineering Summer Meeting, ASME. Miami, USA, 2006.

40. D. Pandya; A low cost micro scale cyclone separator-design and computational fluid dynamics analysis, M. Sc. Thesis, the University of Texas at Arlington. 2010.

41. H. Liu; J. Xu; Ju. Zhang; H. Sun; J. Zhang; Y. Wu.(2012) Oil/water separation in a liquid-liquid cylindrical cyclone. J. Hydrodyn. Ser. B, 24 (1): 116-123.

42. A.F. Najafi; S.M Mousavian; K. Amini.(2011) Numerical investigations on swirl intensity decay rate for turbulent swirling flow in a fixed pipe. Int. J. Mech. Sci., 53 (10) 801~811.

43. S. Wiendelt.(1995) Turbulent pipe flow with swirl. Ph.D. thesis, Eindhoven University of Technology.

44. P. Xu; Z. Wu; A. Mujumdar; B. Yu.(2009) Innovative hydrocyclone inlet designs to reduce erosion-induced wear in mineral dewatering processes. Drying Technol., 27 (2) 201-211.

45. Ansys Fluent 14.5.(2012) Ansys Fluent 14.5 user's Guide, Ansys, Inc.

Fig. 1. Sketch of VAS.

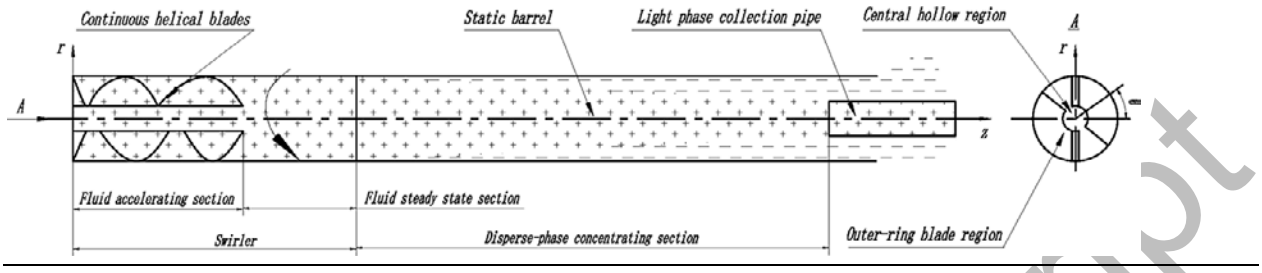

Fig. 2. Structural sketch of the new VAS pilot.

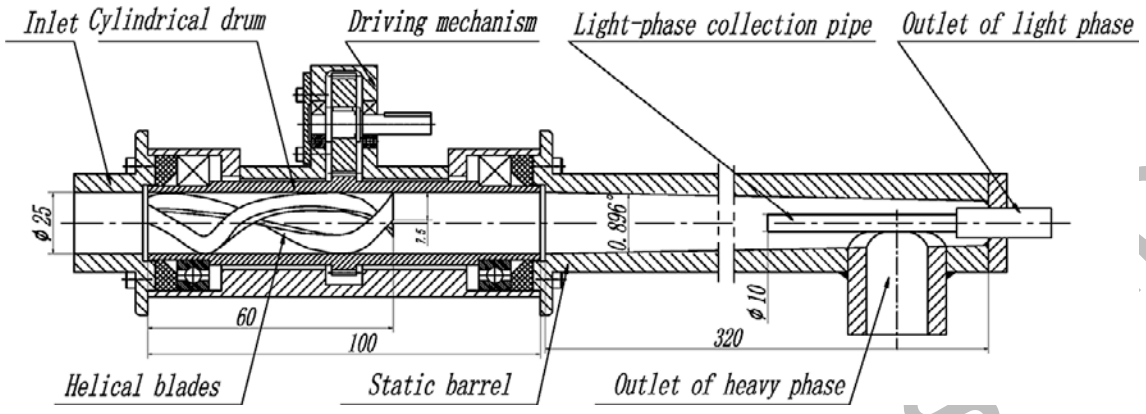

Fig. 3. The sketch development of helical.

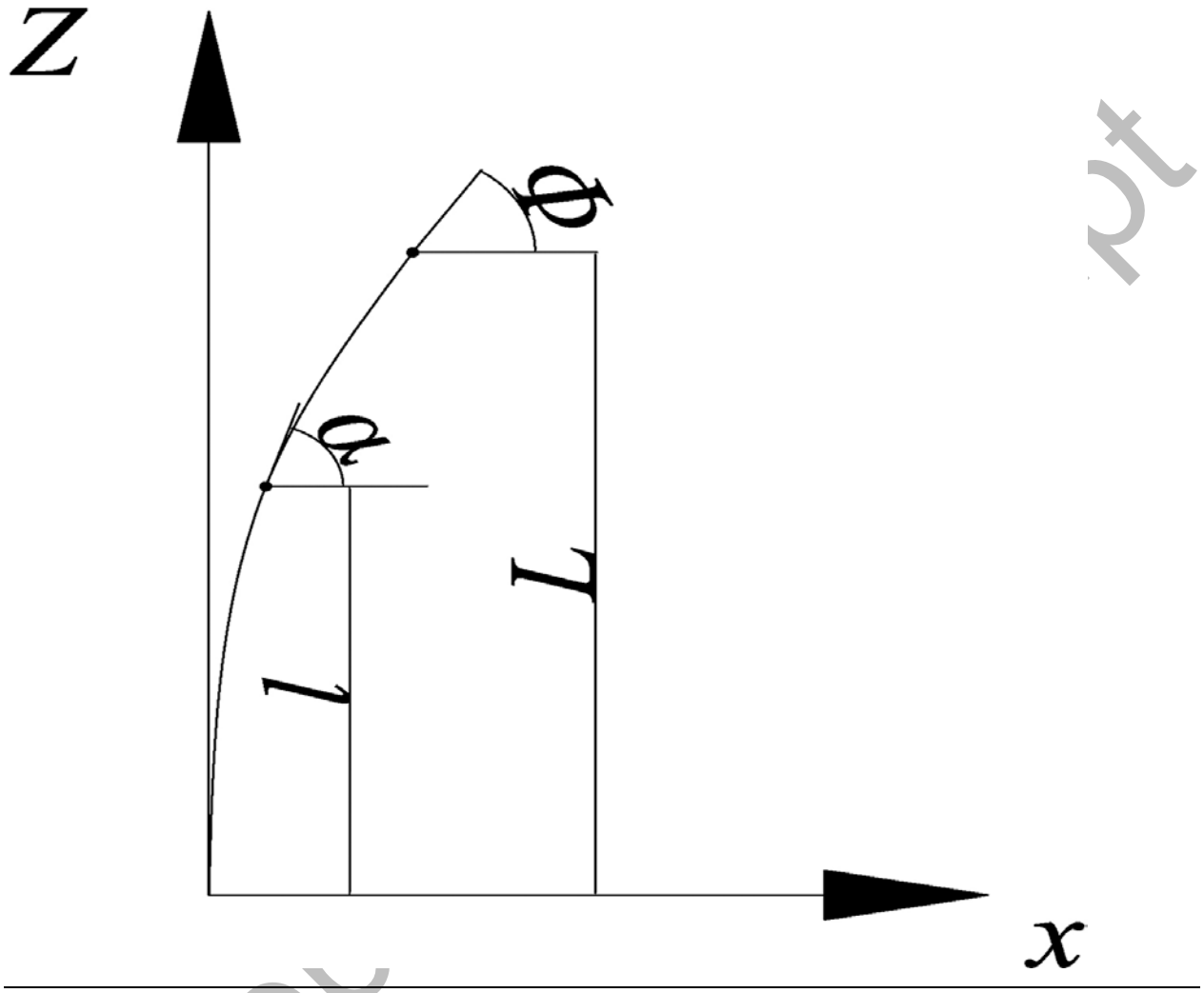

Fig. 4. Distribution diagram of tangential velocity at different positions from drum outlet.

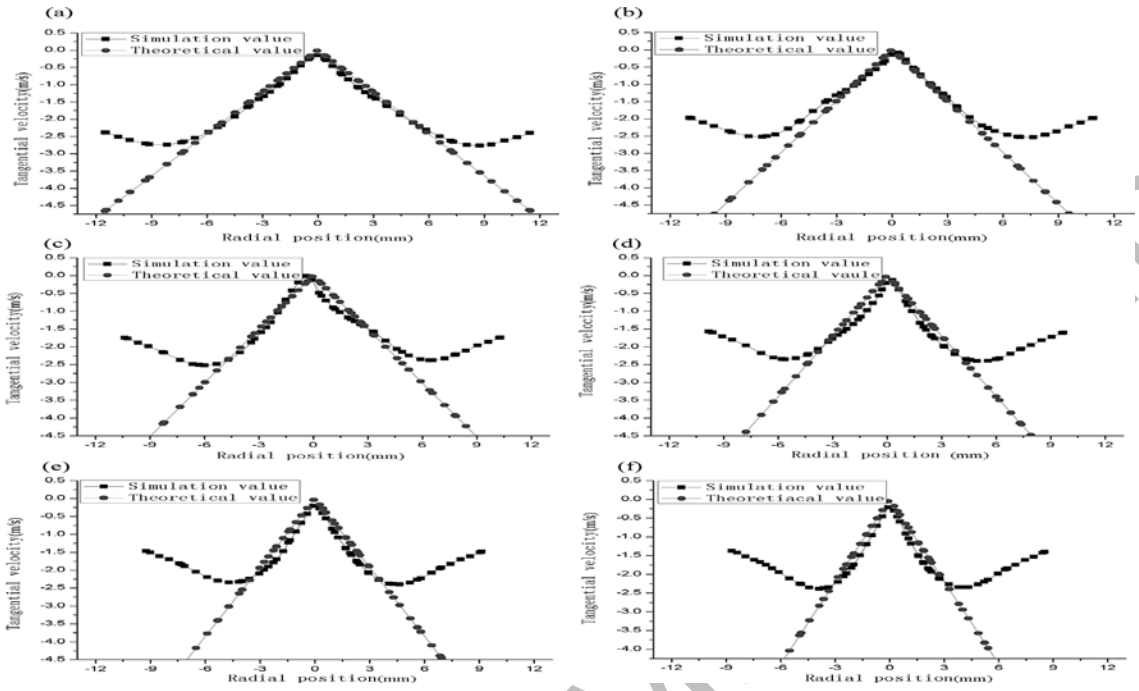


(a) At 50 mm from drum outlet;

(b) At 100 mm from drum outlet;

(c) At 150 mm from the drum outlet;

(d) At 200 mm from the drum outlet;

(e)At 250 mm from the drum outlet;

(f) At 300 mm from the drum outlet.

Fig. 5. Distribution diagram of axial velocity at different positions from drum outlet.

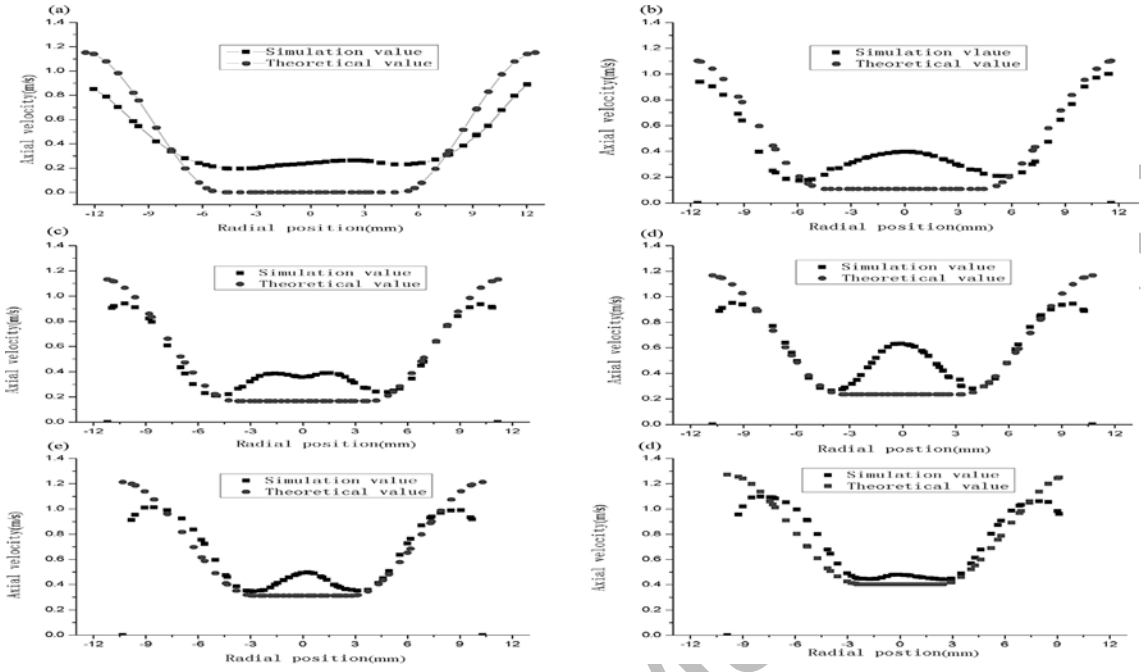


(a) At 50 mm from drum outlet;

(b) At 100 mm from drum outlet;

(c) At 150 mm from the drum outlet;

(d) At 200 mm from the drum outlet;

(e)At 250 mm from the drum outlet;

(f) At 300 mm from the drum outlet.

Fig. 6. The change of separation efficiency with oil droplet size.

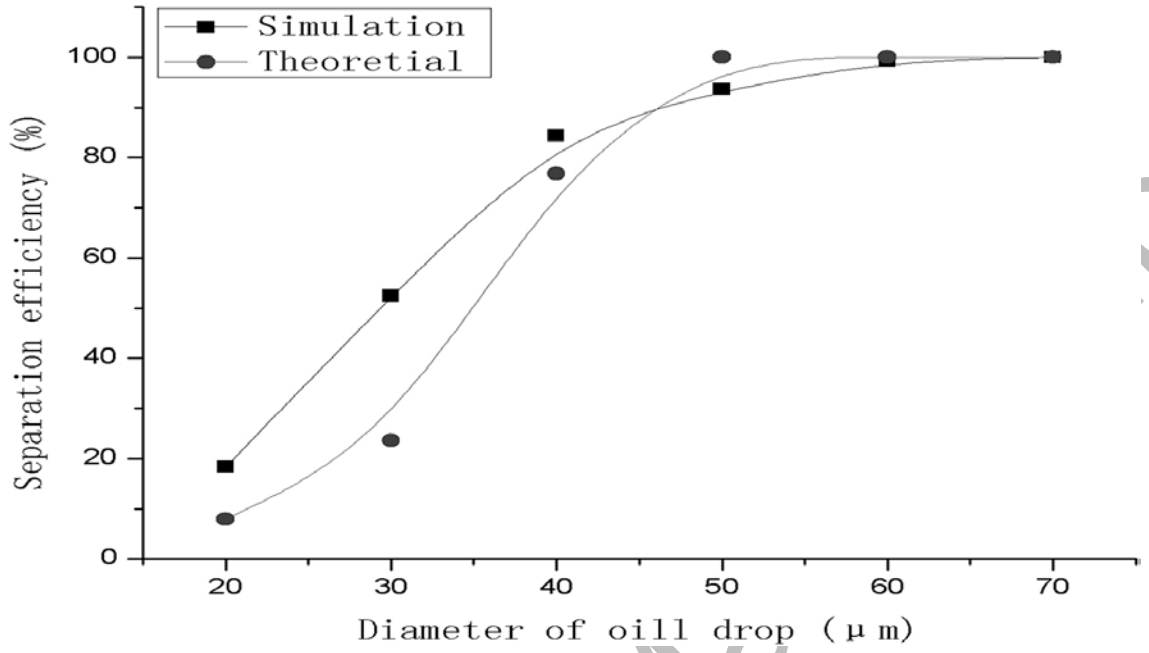

Fig. 7 The relation curves between separation efficiency and back flow ratio.

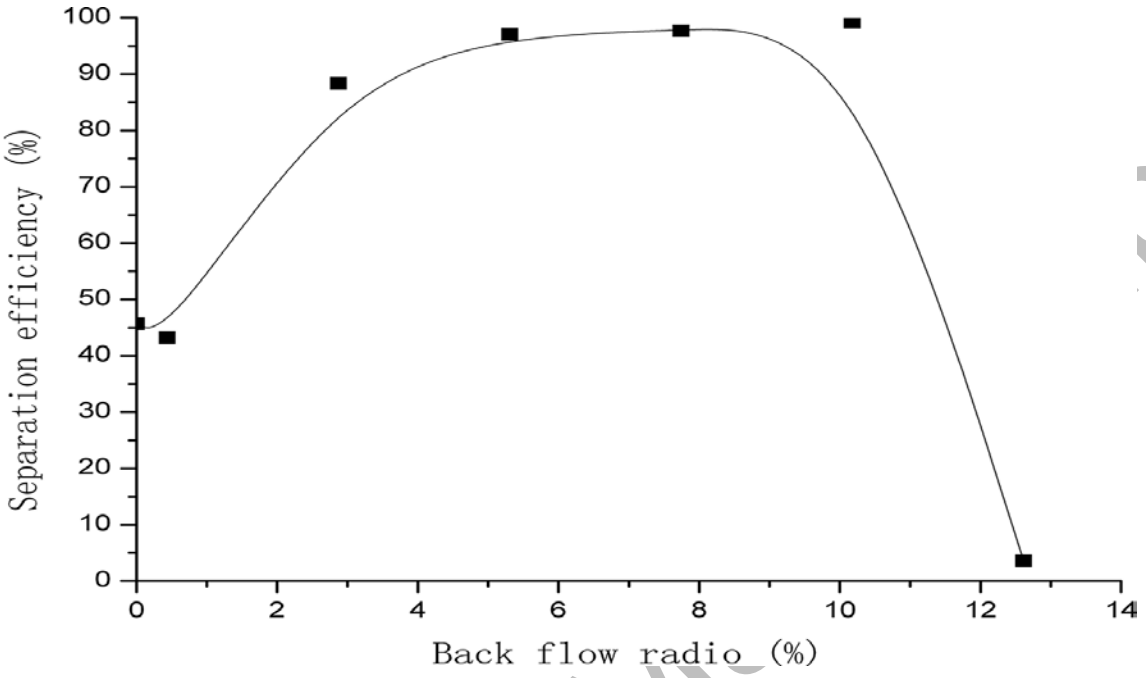

Fig. 8. The distribution of pressure and axial velocity at the outlet of swirler.